nature geoscience

Article

https://doi.org/10.1038/s41561-024-01626-8

Episodic warm climates on early Mars primed by crustal hydration

Received: 16 November 2023

Accepted: 10 December 2024

Published online: 15 January 2025

Check for updates

Danica Adams[1,2] ✉, Markus Scheucher[3], Renyu Hu[2,3], Bethany L. Ehlmann[2], Trent B. Thomas[4], Robin Wordsworth[1,5], Eva Scheller[6], Rob Lillis[7], Kayla Smith[1,8,9], Heike Rauer[10,11] & Yuk L. Yung[2,3]

Geological records indicate that the surface of ancient Mars harboured substantial volumes of liquid water, a resource gradually diminished by processes such as the chemical alteration of crustal materials by hydration and atmospheric escape. However, how a relatively warm climate existed on early Mars to support liquid water under a fainter young Sun is debated. Greenhouse gases such as H_2 in a CO_2-rich atmosphere could have contributed to warming through collision-induced absorption, but whether sufficient H_2 was available to sustain warming remains unclear. Here we use a combined climate and photochemical model to simulate how atmospheric chemistry on early Mars responded to water–rock reactions and climate variations, as constrained by existing observations. We find that H_2 outgassing from crustal hydration and oxidation, supplemented by transient volcanic activity, could have generated sufficient H_2 fluxes to transiently foster warm, humid climates. We estimate that Mars experienced episodic warm periods of an integrated duration of ~40 million years, with each event lasting $\geq 10^5$ years, consistent with the formation timescale of valley networks. Declining atmospheric CO_2 via surface oxidant sinks or variations in the planet's axial tilt could have led to abrupt shifts in the planet's redox state and transition to a CO-dominated atmosphere and cold climate.

Evidence on the surface of present-day Mars suggests that an ~100–1,500 m global equivalent layer of surface liquid water once flowed on Mars during the late Noachian[1,2] for episodes of 10^4–10^6 years over at least 10^8 years (for example, refs. 3–5). A zero-albedo early Mars would have hosted an equilibrium temperature of 210 K, too cold to allow liquid water (for example, ref. 6), suggesting early Mars must have had a thicker atmosphere enriched with greenhouse gases. Reference 7 finds that CO_2 alone, regardless of mass, is unable to sufficiently warm the climate. Collision-induced absorption (CIA) of CO_2 with CH_4 and H_2, due to both transient-induced dipole and dimer effects, could provide sufficient climate forcing to allow liquid water on the early Martian surface[8,9]. However, H_2 can escape to space or be removed by photochemical processes in an oxidized CO_2 atmosphere, and thus requires continuous production to sustain warm conditions. Multiple lines of evidence suggest that crustal hydration and oxidation was a significant source of H_2 in the early atmosphere (for example, refs. 10–13), but to date the effect of this process on atmospheric chemistry and climate has not been examined in detail.

[1]Department of Earth and Planetary Sciences, Harvard University, Cambridge, MA, USA. [2]Division of Geological and Planetary Sciences, California Institute of Technology, Pasadena, CA, USA. [3]Jet Propulsion Laboratory, California Institute of Technology, Pasadena, CA, USA. [4]Department of Earth and Space Sciences and Astrobiology Program, University of Washington, Seattle, WA, USA. [5]School of Engineering and Applied Sciences, Harvard University, Cambridge, MA, USA. [6]Department of Earth, Atmospheric, and Planetary Sciences, MIT, Cambridge, MA, USA. [7]Space Sciences Laboratory, University of California, Berkeley, CA, USA. [8]Central State University, Wilberforce, OH, USA. [9]Department of Planetary Sciences, Lunar and Planetary Sciences, University of Arizona, Tucson, AZ, USA. [10]Freie Universitat, Berlin, Germany. [11]German Aerospace Center (DLR), Berlin, Germany. ✉e-mail: dadams@fas.harvard.edu

https://doi.org/10.1038/s41561-024-01626-8

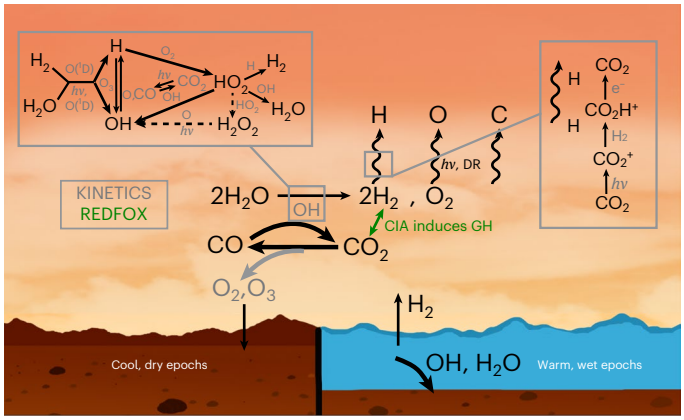

Fig. 1 | Mars H, C, O chemistry including ground sinks and escape processes. Cartoon is split into two epochs: warm, wet (with crustal hydration and oxidation releasing H_2) and cold, dry (with oxidants lost to oxidizing reduced iron near the surface). In all epochs, CO_2 and H_2O photolysis (energy from photons represented in the cartoon as *hν*) drives the photochemistry, and escape of H, C and O is considered. At Mars today, dissociative recombination (DR) is the main process for oxygen escape.

A comprehensive photochemical evolution and climate model

We developed a new combined model of climate and photochemistry on early Mars, including effects of all H, C and O sinks (Methods, 'Photochemical model'). This model simulates the change in atmospheric redox and chemistry in response to near-surface water–rock reactions and climate variations while providing constraints on the timescales of such redox changes. It allows us to investigate how atmospheric and crustal sinks, combined, controlled early Mars' atmospheric chemistry and climate, advancing beyond previous work that focused on climate and bulk redox effects[8,14].

We adapt KINETICS, the Caltech/Jet Propulsion Laboratory one-dimensional (1D) photochemical and transport model[15] (Methods, 'Photochemical model'), to consider an initial set of six atmospheric pressures and bulk compositions for early Mars: surface pressures of 200 mbar–1.3 bar of background CO_2 and varied N_2 contents of up to 300 mbar. This set spans likely atmospheric variation during the Noachian and Hesperian periods and uncertainty in N_2/CO_2 composition[16]. Our upper limits are motivated by isotope evolution models and recent measurements (Methods, 'Photochemical model').

We consider two scenarios for each of the potential atmospheres: with and without surface liquid water. (1) For those with near-surface liquid water, we explore a set of hydrogen fluxes of 10^9–10^{12} cm^{-2} s^{-1} H_2, a wide range motivated by the uncertainty of several terms, including H_2 released per H_2O lost, depth of oxidation and hydration, potential for episodically faster or slower releases of hydrogen from crustal hydration and potential for transient volcanic activity. (2) For those without near-surface liquid water, we range the dry oxidant sinks as a free parameter across 10^6–10^9 cm^{-2} s^{-1} O_2. In all cases, these hydration/oxidation fluxes enter our atmospheric model at the lower boundary at a prescribed rate for each case. Although the oxidation loss may be kinetically inhibited, several works identify a similar mechanism probably occurred at early Earth (for example, refs. 17,18).

Our model considers atmospheric chemical production and loss, vertical transport with both molecular and eddy diffusion, and at the boundary conditions, fluxes or velocities of species as needed into or out of the atmosphere. The main chemical networks are demonstrated in Fig. 1 and described in the following sections. We solve for atmospheric escape of H, C and O (Methods, 'Photochemical model'). We fix the water-vapour profile to saturation vapour pressure below the hygropause and in higher altitudes assign a constant mixing ratio (for the cold-trapped layers; Methods, 'Photochemical model'). We ignore the effect of dust storms, but we acknowledge their inclusion would increase the H escape rate on short timescales (less than one Mars year per event). MAVEN (Mars Atmosphere and Volatile Evolution Mission) measurements suggest up to 5–10× increases in hydrogen escape rates during dust storms (for example, refs. 19,20), although the frequency and effect of dust storms in earlier climates and thicker atmospheres is not well constrained.

We iterate KINETICS with REDFOX, a correlated-*k* radiative–convective 1D climate module[21] that we use to solve for the temperature profiles at pressures larger than 1 μbar. REDFOX includes CIA of H_2–H_2, CO_2–H_2, CO_2–CH_4 and CO_2–CO_2, as well as Mlawer–Tobin–Clough–Kneizys–Davies water-vapour continuum model for H_2O continuum absorption. We add N_2–H_2 CIA to REDFOX for this study.

A sustained source of atmospheric H_2 from crustal hydration

For each surface pressure, the steady-state H_2 mixing ratios range over orders of magnitude, reaching less than 1 ppm in the cases with only photochemistry and reaching up to 17% in the cases with surface fluxes of 2×10^{12} H_2 cm^{-2} s^{-1} (Fig. 2). Because the range of H_2 fluxes is the same across all surface pressures, a larger surface pressure dilutes the mixing ratio of H_2. However, H_2 mixing ratio does not scale linearly with surface pressure because diffusion and escape is slower in a thicker atmosphere. In all cases, the timescale of diffusion-limited escape (~10^5 years) controls the lifetime of H_2 build-up and removal and governs the steady-state abundance of H_2 in the lower atmosphere. Thus in the set of simulations assuming crustal hydration, oxidation and volcanic H_2 fluxes, if the H_2 fluxes persist for >10^5 years, we find notably increased steady-state H_2 abundances.

In agreement with refs. 8,9, we find that H_2 mixing ratios of several percent and larger are required to warm the global mean average surface temperature above 270 K in the 1 bar atmosphere. In our model, the following cases are able to warm the climate above 250 K (upper panels; Fig. 2), which probably could have supported local surface liquid water[22]: 2×10^{12} H_2 cm^{-2} s^{-1} flux in 800 mbar, 1 bar and 1.3 bar atmospheres; and 1×10^{12} H_2 cm^{-2} s^{-1} in the 1 bar and 1.3 bar atmospheres.

Geologic constraints on crustal H_2 release

Iron oxidation and crustal hydration together sequestered ~100–900 m global equivalent layer of liquid water (GEL) and ~10–100 m GEL during the Noachian and Hesperian periods, respectively, primarily as Fe/Mg phyllosilicates[13]. We treat the two water sink processes differently in modelling and later sum to estimate fluxes of hydrogen of geologic origin into the atmosphere: (1) Fe(II) oxidation to Fe(III) and (2) water lost to forming hydrated minerals. (1) Water loss to iron oxidation, the first scenario, occurs primarily by electron transfer between Fe and H and can be summarized as the following redox reaction (for example, ref. 12):

$$2\,FeO + H_2O \longleftrightarrow Fe_2O_3 + H_2$$

To determine the flux of hydrogen release, we base the same assumptions on reaction depths as ref. 13: ~5–10 km in the Noachian and ~1–5 km in the Hesperian. In addition[23], show that typical Martian basalt contains 20 wt% FeO (both Fe(II) and Fe(III)) and that $Fe^{3+}/Fe^{T} < 0.2$–0.3 for relatively unaltered basalts on Mars and 0.6–0.9 for highly altered basalts. Assuming 10–60% of all Fe(II) in basalt was oxidized to Fe(III), this yields a range of H_2 released by iron oxidation expressed as a water equivalent volume: 30–380 m GEL during the Noachian and 6–190 m GEL during the Hesperian. (2) During crustal hydration, clay minerals and other hydrated minerals incorporate OH groups and H_2O groups, and only the former will release hydrogen. The ratio of OH groups incorporated per H_2O group lost is extremely variable from mineral to mineral. Following ref. 11 and their literature review of serpentine, we assume an H_2O-in/H_2-out ratio range of ~4–40. While Mars does

https://doi.org/10.1038/s41561-024-01626-8

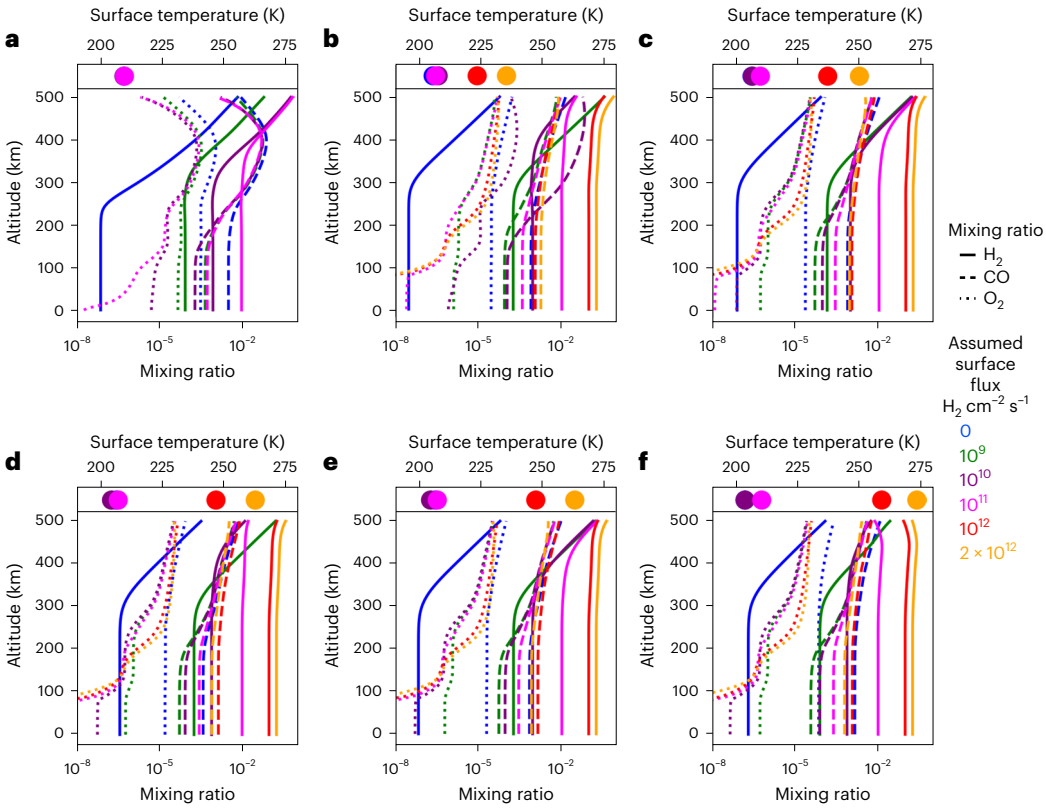

Fig. 2 | Surface temperatures and steady-state chemistry in cases with crustal hydration. a–**f**, Mixing ratio (dimensionless) profiles of H_2 (solid), O_2 (dots) and CO (dashed) in five atmospheres: 200 mbar 90% CO_2 (**a**), 500 mbar 90% CO_2 (**b**), 800 mbar 62% CO_2 (**c**), 1 bar 90% CO_2 (**d**), 1 bar 75% CO_2 (**e**) and 1.3 bar 75% CO_2 (**f**). The complementary component of the atmosphere is N_2. We assume the 200 mbar atmosphere would correspond to the Hesperian period; therefore, we consider only a lower range of sinks in this case. Surface temperatures (K) are shown in insets at the top of each panel following the same colour scheme. Models shown are run to steady state (>10^8 years, after which there is negligible variation in species concentration over time). In the text, mixing ratio is described in units of percentage (where 100% is a mixing ratio of 1).

not show widespread serpentine, we use the serpentine Fe/Mg phyllosilicate group range simply due to lack of such ratios for similar and commonly detected Martian Fe/Mg smectites[24,25] that also generate H_2 (ref. 12). From this, we obtain a range of H_2 released by crustal hydration expressed as volume of water equivalent: 4–400 m GEL during the Noachian and 0.4–44 m GEL during the Hesperian. By summing these two scenarios and averaging over the full lengths of the Noachian and Hesperian periods, respectively, this suggests a hydrogen flux of ~10^9–10^{11} H_2 cm^{-2} s^{-1}.

Our results in Fig. 2 show that a hydrogen flux of only 10^{12} H_2 cm^{-2} s^{-1} or larger may sustain a warm climate. Planetary crustal H_2 fluxes of this magnitude agree with some previous work[12,26] while others[14] invoked intermittent geologic events to motivate such large fluxes (Methods, 'Photochemical model'). Therefore, our results demonstrate that although crustal hydration can provide sustained warm climates, periods of faster crustal hydration and greater H_2 flux than the average over geologic history are required to result in a warm climate. If crustal hydration occurred at 10^{12} H_2 cm^{-2} s^{-1}, it could not have been for longer than ~4×10^7 years cumulatively; any longer would have required too much water (more than the upper limit of 900 m GEL) to have been lost to the crust. (This conclusion is determined by solving for the duration of water loss required to relate the metres GEL lost in the two scenarios described in the preceding to a hydrogen flux of 10^{12} H_2 cm^{-2} s^{-1}).

Three scenarios could explain episodically faster rates of crustal hydration. (1) While Mars was probably not warm during the full Noachian, crustal hydration may have continued to occur in the subsurface, where the temperature is controlled largely by the geotherm. This process would have produced hydrogen, but if covered by an ice layer the hydrogen may have built up while being stored in the subsurface. Melting or sublimation of the ice may have released the built-up hydrogen at faster rates than the time average. Previous works have considered similar processes for release of methane from clathrates[9,27]. (2) Crustal hydration by definition requires the altering of fresh crust, which was probably supplied by volcanism. Following a volcanic event, larger volumes of fresh material may have been available for alteration, and the formation of this crust may have taken up to hundreds of thousands of years or longer. (3) Volcanism itself may have transiently released large fluxes of H_2 (refs. 28,29). Figure 3 shows that hydrogen from a single event would leave the atmosphere through diffusion-limited escape on timescales of ~10^5 years. Like ref. 28, we estimate ~1×10^{10} H_2 cm^{-2} s^{-1} is an upper limit of the time-averaged H_2 outgassing, assuming a reduced mantle (IW-1) and a magma H_2O content of 0.2 wt% (Earth's mid-ocean ridge basalt). This rate suggests volcanism could have an additive effect in transiently warming the climate, but warming effects may have been more episodic than crustal release (the latter has a larger time-averaged maximum release of H_2). The additive effect of volcanism is important, and transient volcanic events also could have helped trigger episodes of faster crustal hydration (for example, scenarios 1 + 2). In summary, our results suggest that Mars's climate could only have been warm for a cumulative duration of up to 4×10^7 years (if releasing 10^{12} H_2 cm^{-2} s^{-1}) and that each warm event would have endured ~10^5 years.

Photochemically unstable CO_2 under cool and dry climates

In putative cool, dry epochs, little to no surface water would have been available, and therefore, water–rock reactions sourcing H_2 would

https://doi.org/10.1038/s41561-024-01626-8

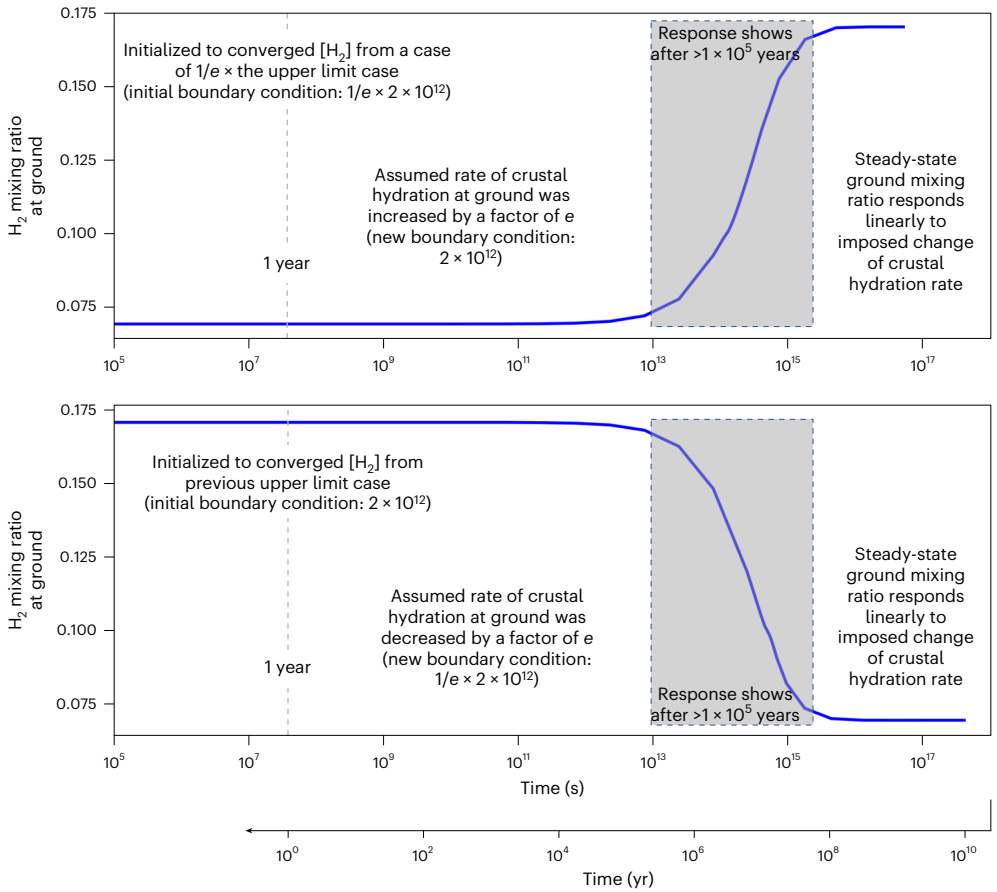

Fig. 3 | Lifetime of near-surface hydrogen. Temporal response of the near-surface mixing ratio of H_2 to factor of *e* (Euler's number, ~2.7) variations in the assumed crustal hydration rate for release of H_2 into the atmosphere. We find a lifetime of ~10^5 years when both increasing (upper panel) and decreasing (lower panel) this rate.

slow or cease, leaving only episodic volcanism as a potential source. Nonetheless, slower atmospheric oxidation of Fe(II) igneous minerals near the surface may have still occurred, a scenario previously considered by ref. 30. We vary the crustal sink of oxygen from 10^6 cm^{-2} s^{-1} to 10^9 cm^{-2} s^{-1}, with a lower bound representing a flux with negligible influence on the atmospheric chemistry and an upper bound within the range of oxidative weathering considered by ref. 30. Our upper bound of 10^9 O_2 cm^{-2} s^{-1} corresponds to ~7 m oxidation over ~600 million years (approximately the duration of the Noachian). We turn off all aqueous processes. Our boundary conditions include no source of crustal H_2 release at the lower boundary and no aqueous deposition of CO or HNO_x species. Additional sensitivity studies are given in Methods, 'Photochemical model'.

When ground sinks of atmospheric oxygen are introduced, we find that the hydrogen escape rate increases. The loss of hydrogen to water in a 2/1 ratio occurs while the system has sufficient water vapour to source OH and balance the atmospheric oxygen sinks to the crust. However, once the assumed crustal oxidant sinks are increased beyond a rate that the modelled hydrogen diffusion can match (near ~10^9 cm^{-2} s^{-1}), the hydrogen escape rate can no longer increase to balance the assumed crustal oxygen sinks. Instead, oxygen pulled off of CO_2 (from photolysis) must source the oxidant sink, since water photolysis supplies O slower than the oxidant sink. This causes the CO mixing ratio to rise (Fig. 3) and places a ceiling on H escape such that H/O escape is no longer in an ~2/1 ratio. Our model with updated photochemical parameterization for loss of carbon and coupling to a 1D climate model thus comes to a similar result as ref. 30: high-oxidant sinks result in a CO runaway in initially thick CO_2-dominated atmospheres.

Figure 4 shows that the CO runaway takes at least 10^7 years to build up. We hypothesize two possible mechanisms to destroy or prevent a CO-dominated atmosphere. Geologic events such as obliquity changes or volcanism could have episodically released H_2 (or other species) and warmed the atmosphere before the CO_2 ran away to CO, thereby slowing the onset of the CO runaway. During warm climates, the saturation vapour pressure of water is higher, which causes greater availability of OH. Loss of atmospheric oxygen to surface iron may also decrease during warm climates: surface waters may oxidize the iron, after which point O_2 dissolution into waters would be in equilibrium and draw down O_2 at a relatively lower rate. Second, convective and dynamical processes could have transported water to the upper atmosphere, allowing rapid H escape and production of oxygen for interaction with the surface. We investigate the effects of such water transport in our 1D model but find the oxidation of the surface outpaces this in general (Supplementary Table 1).

In contrast with these results, present-day Mars has a photochemically stable CO_2 atmosphere. Over Mars's history, the surface iron becomes largely oxidized, sinks of atmospheric oxidants to the ground slow, and H escape takes over again to return the atmosphere to CO_2 dominance. That is, the rate of physical weathering to expose new materials for weathering is less than the rate of chemical oxidative weathering. Therefore, iron oxidation minimally impacts the atmospheric chemistry, and CO_2 is photochemically stable at present-day Mars.

Catalytic chemistry involving chlorine radicals is known to prevent a CO runaway at Venus (for example, ref. 31), but the CO runaway problem is not unique to early Mars and has also been studied for exoplanets around M-dwarf stars (for example, refs. 32,33). Including Cl chemistry is beyond the scope of this work (Methods, 'Photochemical model').

https://doi.org/10.1038/s41561-024-01626-8

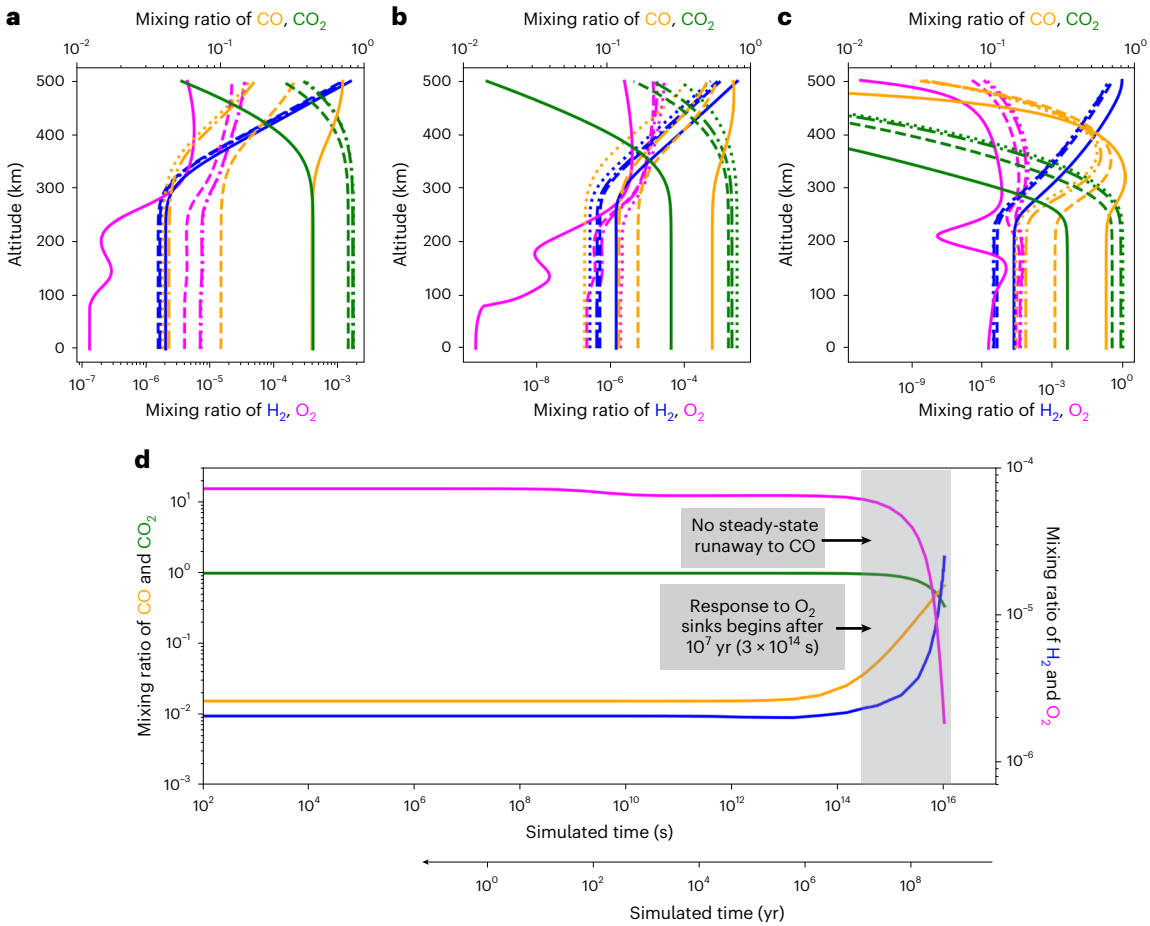

Fig. 4 | Mixing ratio outputs from cold early Mars cases. a–c, Mixing ratio profiles of H_2 (blue), O_2 (magenta), CO (orange) and CO_2 (green) in three atmospheres: 1 bar, 90% CO_2 (**a**), 500 mbar, 90% CO_2 (**b**) and 200 mbar, 90% CO_2 (**c**). For all cases, the ranges of oxidant ground sinks shown are as follows: 0 (dots), 10^7 cm^{-2} s^{-1} (dash dot), 10^8 cm^{-2} s^{-1} (dashed). We vary the upper limit (solid) as a function of surface pressure: 10^9 cm^{-2} s^{-1} (1 bar), 5×10^8 (500 mbar), 2×10^8 (200 mbar). Models are run for the duration of the Noachian era (400 Myr), and the resulting profiles after 400 Myr are shown. **d**, Response of mixing ratio of CO and CO_2 (left axis) and H_2 and O_2 (right axis) over time to an introduced sink of atmospheric O_2 into the ground.

Implications for early Mars's climate and redox chemistry

Our coupled photochemical–climate model finds two plausible chemical and climate states for early Mars on long timescales: (1) a warm climate capable of sustaining surface liquid water for 10^5–10^7 years by large mixing ratios of H_2 supplied by crustal hydration (Fig. 2); (2) an early cool climate lasting >10^7 years with runaway to a cooler, CO-dominated atmosphere via oxidant sinks to the surface (Fig. 4). The timescale we find for the former is in approximate agreement with geochemical analyses and geomorphologic features, which suggest surface liquid water probably cumulatively interacted with the surface for ~10^5–10^7 years over Mars's early history[1,4,24,34–37].

Mars's atmosphere may not always have been in chemical steady state, so these two solutions are endmember cases. It is plausible that Mars's atmosphere underwent abrupt redox changes by alternating from highly oxidized (CO_2-rich), to mildly reduced (CO_2–H_2) and warm, and to reduced and cold (CO-dominant). Our chemical model provides constraints on the minimum lifetime of each climate. We find that the timescale for atmospheric H_2 build-up or removal to begin is ~10^5 years, and steady state is reached near ~10^7 years (shown in Fig. 3). The former timescale probably describes the minimum duration for each warm CO_2–H_2 period. Our model also suggests crustal hydration could not have warmed the climate for longer than a cumulative total time of ~$2–4 \times 10^7$ years (depending on the atmospheric pressure, corresponding to about 10% of the Noachian period), unless the present-day water inventory contained in the ice and the crust[13] is underestimated. Therefore, our results imply only a few major warming events (~1 to 100 events, each of 10^5–4×10^7 years in duration).

Evidence for our hypothesis of alternating redox states is supported by several recent observations. First, Mars's surface has a paucity of surface carbonates (for example, ref. 25), which are expected to form in the presence of neutral pH water and a CO_2-dominated atmosphere with extensive open-system crustal alteration at the surface. If under different atmospheric conditions where the duration of the warm climates is short, our hypothesis can explain the global lack of carbonates[24]. Second, a reducing CO-dominated atmosphere may also help to explain ~3.5 billion-year-old sedimentary organic carbon at Gale crater that is depleted in ^{13}C by ~100‰ compared with the atmosphere (for example, refs. 38,39).

Mars's surface rocks contain both reduced species, including trichloromethane[40], H_2S (refs. 40,41) and nitriles[42], and oxidized species, including perchlorate[40,43], nitrate[41–43] and sulfate[43], which suggests the surface of Mars is far from equilibrium. While both oxidized and reduced species may form under one climate, the deposition rate of different species is sensitive to the climate. For example, warm climates preferentially deposit nitrate[44] while cool climates preferentially deposit nitrite[45,46]. The steady-state photochemical results of this work are thus endmember cases of the varying redox states Mars may have experienced through time, analogous to Earth's redox history although with different drivers.

Finally, Mars's interior may have become more oxidizing with time (for example, refs. 47,48). Considering this evolution would be particularly important for understanding the flux of gases that act as episodic perturbers to more steady-state CO_2-rich, mildly reduced (CO_2–H_2) and warm, and reduced and cold (CO-dominant) conditions. Hence, full interpretation of the redox paradox will require careful comparison of our alternating atmospheric redox hypothesis with chemical and isotopic datasets collected in situ and with igneous and water-altered rocks from the first 1–2 billion years of Mars history that comprise the samples presently being collected by the Perseverance rover.

Online content

Any methods, additional references, Nature Portfolio reporting summaries, source data, extended data, supplementary information, acknowledgements, peer review information; details of author contributions and competing interests; and statements of data and code availability are available at https://doi.org/10.1038/s41561-024-01626-8.

References

1. Carr, M. H. & Head, J. W. Oceans on Mars: an assessment of the observational evidence and possible fate. *J. Geophys. Res. Planets* https://doi.org/10.1029/2002JE001963 (2003).
2. Clifford, S. M. & Parker, T. J. The evolution of the Martian hydrosphere: implications for the fate of a primordial ocean and the current state of the northern plains. *Icarus* **154**, 40–79 (2001).
3. Barnhart, C., Howard, A. & Moore, J. Long-term precipitation and late-stage valley network formation: landform simulations of Parana Basin, Mars. *J. Geophys. Res.* **114**, E01003 (2009).
4. Hoke, M., Hynek, B. & Tucker, G. Formation timescales of large Martian valley networks. *Earth Planet. Sci. Lett.* **312**, 1–12 (2011).
5. Schon, S., Head, J. & Fassett, C. An overfilled lacustrine system and progradational delta in Jezero crater, Mars: implications for Noachian climate. *Planet. Space Sci.* **67**, 28–45 (2012).
6. Wordsworth, R. The climate of early Mars. *Annu. Rev. Earth Planet. Sci.* **44**, 381–408 (2016).
7. Pollack, J., Kasting, J., Richardson, S. & Poliakoff, K. The case for a wet, warm climate on early Mars. *Icarus* **71**, 203–224 (1987).
8. Ramirez, R. et al. Warming early Mars with CO_2 and H_2. *Nat. Geosci.* **7**, 59–63 (2014).
9. Wordsworth, R. et al. Transient reducing greenhouse warming on early Mars. *Geophys. Res. Lett.* **44**, 665–671 (2017).
10. Chassefiere, E. & LeBlanc, F. Constraining methane release due to serpentinizaton by the observed D/H ratio on Mars. *Earth Planet. Sci. Lett.* **310**, 3–4 (2011).
11. Chassefiere, E. et al. The fate of early Mars' lost water: the role of serpentinization. *J. Geophys. Res. Planets* **118**, 1123–1134 (2013).
12. Tosca, N. J. et al. Magnetite authigenesis and the warming of early Mars. *Nat. Geosci.* **11**, 635–639 (2018).
13. Scheller, E., Ehlmann, B., Hu, R., Adams, D. & Yung, Y. Long-term drying of Mars by sequestration of ocean-scale volumes of water in the crust. *Science* **372**, 56–62 (2021).
14. Wordsworth, R. et al. A coupled model of episodic warming, oxidation and geochemical transitions on early Mars. *Nat. Geosci.* **14**, 127–132 (2021).
15. Allen, M., Yung, Y. L. & Waters, J. W. Vertical transport and photochemistry in the terrestrial mesosphere and lower thermosphere (50–120 km). *J. Geophys. Res. Space Phys.* **86**, 3617–3627 (1981).
16. Hu, R. & Thomas, T. A nitrogen-rich atmosphere on ancient Mars consistent with isotopic evolution models. *Nat. Geosci.* **15**, 106–111 (2022).
17. Payne, R. C., Brownlee, D. & Kasting, J. F. Oxidized micrometeorites suggest either high p_{CO_2} or low p_{N_2} during the Neoarchean. *Proc. Natl Acad. Sci. USA* **117**, 1360–1366 (2020).
18. Tomkins, A. et al. Ancient micrometeorites suggestive of an oxygen-rich Archaean upper atmosphere. *Nature* **533**, 235–238 (2016).
19. Heavens, N. et al. Hydrogen escape from Mars enhanced by deep convection in dust storms. *Nat. Astron.* **2**, 126–132 (2018).
20. Chaffin, M. et al. Martian water loss to space enhanced by regional dust storms. *Nat. Geosci.* **5**, 1036–1042 (2021).
21. Scheucher, M. et al. Consistently simulating a wide range of atmospheric scenarios for K2-18b with a flexible radiative transfer module. *Astrophys. J.* **898**, 44 (2020).
22. Ramirez, R., Craddock, R. & Usui, T. Climate simulations of early Mars with estimated precipitation, runoff, and erosion rates. *J. Geophys. Res. Planets* **125**, e2019JE006160 (2020).
23. Morris, R. V. et al. Mössbauer mineralogy of rock, soil, and dust at Gusev crater, Mars: spirit's journey through weakly altered olivine basalt on the plains and pervasively altered basalt in the Columbia Hills. *J. Geophys. Res. Planets* https://doi.org/10.1029/2005JE002584 (2006).
24. Ehlmann, B. et al. Subsurface water and clay mineral formation during the early history of Mars. *Nature* **479**, 53–60 (2011).
25. Ehlmann, B. & Edwards, C. Mineralogy of the Martian surface. *Annu. Rev. Earth Planet. Sci.* **42**, 291–315 (2014).
26. Merdith, A. et al. Pulsated global hydrogen and methane flux at mid-ocean ridges driven by Pangea breakup. *Geochem. Geophys. Geosyst.* **21**, e2019GC008869 (2020).
27. Kite, E., Mischna, M., Gao, P., Yung, Y. & Turbet, M. Methane release on early Mars by atmospheric collapse and atmospheric reinflation. *Planet. Space Sci.* **181**, 104820 (2020).
28. Thomas, T., Hu, R. & Lo, D. Constraints on the size and composition of the ancient Martian atmosphere from coupled CO_2–N_2–Ar isotopic evolution models. *Planet. Sci. J.* **4**, 41 (2023).
29. Wadhwa, M. Redox state of Mars' upper mantle and crust from Eu anomalies in shergottite pyroxenes. *Science* **291**, 1527–1530 (2001).
30. Zahnle, K., Haberle, R., Catling, D. & Kasting, J. Photochemical instability of the ancient Martian atmosphere, *J. Geophys. Res.* https://doi.org/10.1029/2008JE003160 (2008).
31. Yung, Y. & Demore, W. Photochemistry of the stratosphere of Venus: implications for atmospheric evolution. *Icarus* **51**, 199–247 (1982).
32. Hu, R., Peterson, L. & Wolf, E. O_2 and CO-rich atmospheres for potentially habitable environments on Trappist-1 planets. *Astrophys. J.* **888**, 122 (2020).
33. Christensen, M., Adams, D., Wong, M., Dunn, P. & Yung, Y. New estimates of nitrogen fixation on early Earth. *Life* **14**, 601 (2024).
34. Lapotre, M. & Ielpi, A. The pace of fluvial meanders on Mars and implications for the western delta depositions of Jezero crater. *AGU Adv.* **1**, e2019AV000141 (2020).
35. Olsen, A. A. et al. Using a mineral lifetime diagram to evaluate the persistence of olivine on Mars. *Am. Mineral.* **92**, 598–602 (2007).
36. Bishop, J. et al. Surface clay formation during short-term warmer and wetter conditions on a largely cold ancient Mars. *Nat. Astron.* **2**, 206–208 (2018).
37. Grotzinger, J. et al. Deposition, exhumation, and paleoclimate of an ancient lake deposit, Gale crater, Mars. *Science* **350**, aac7575 (2015).
38. Yoshida, T. et al. Strong depletion of ^{13}C in CO induced by photolysis of CO_2 in the Martian atmosphere, calculated by a photochemical model. *Planet. Sci. J.* **4**, 53 (2023).
39. House, C. et al. Depleted carbon isotope compositions observed at Gale crater, Mars. *Proc. Natl Acad. Sci. USA* **119**, e2115651119 (2022).
40. Glavin, P. et al. Evidence for perchlorates and the origin of chlorinated hydrocarbons detected by SAM at the Rocknest aeolian deposit in Gale Crater. *J. Geophys. Res. Planets* **113**, 1955–1973 (2013).

41. Stern, J. et al. Evidence for indigenous nitrogen in sedimentary and aeolian deposits from the Curiosity rover investigations at Gale crater, Mars. *Proc. Natl Acad. Sci. USA* **112**, 4245–4250 (2015).
42. Stern, J. et al. Major volatiles evolved from eolian materials in Gale crater. *Geophys. Res. Lett.* **45**, 10,240–10,248 (2018).
43. Sutter, B. et al. Evolved gas analyses of sedimentary rocks and eolian sediment in Gale crater, Mars: results of the Curiosity rover's sample analysis at Mars instrument from Yellowknife Bay to the Namib Dune. *J. Geophys. Res. Planets* **122**, 2574–2609 (2017).
44. Adams, D. et al. Nitrogen fixation at early Mars. *Astrobiology* **21**, 968–980 (2021).
45. Adams, D. et al. Nitrogen fixation at paleo-Mars in an icy atmosphere. *Geophys. Res. Lett.* **51**, e2024GL111063 (2024).
46. Catling, D. et al. Atmospheric origins of perchlorate on Mars and in the Atacama. *J. Geophys. Res.* https://doi.org/10.1029/2009JE003425 (2010).
47. Wade, J. & Wood, B. Core formation and the oxidation state of the Earth. *Earth Planet. Sci. Lett.* **236**, 78–95 (2005).
48. Grott, M., Morschhauser, A., Breuer, D. & Hauber, E. Volcanic outgassing of CO_2 and H_2O on Mars. *Earth Planet. Sci. Lett.* **308**, 391–400 (2011).

Publisher's note Springer Nature remains neutral with regard to jurisdictional claims in published maps and institutional affiliations.

Springer Nature or its licensor (e.g. a society or other partner) holds exclusive rights to this article under a publishing agreement with the author(s) or other rightsholder(s); author self-archiving of the accepted manuscript version of this article is solely governed by the terms of such publishing agreement and applicable law.

© The Author(s), under exclusive licence to Springer Nature Limited 2025

Methods

Photochemical model

We adapt the Caltech/Jet Propulsion Laboratory photochemical and transport model, KINETICS, for the early Mars atmosphere. Additional input and output files from our study can be found in the Data Availability statement. The KINETICS software is described in the original references[15,49], and the work can be reproduced with all reactions and rate constants used in this study, which are included in the provided output files. We consider the chemistry of 28 species linked by 172 reactions on an altitude grid spaced on average with three bins per scale height that extends to 500 km (well above the exobase for our five atmospheric pressures considered). Our model calculates and outputs chemical abundances for each species at every level by computing the chemical production and loss rates at each altitude as well as the diffusive flux between each altitude grid with the 1D continuity equation:

$$\frac{\mathrm{d}n_i}{\mathrm{d}t} = P_i - L_i - \frac{\partial \phi_i}{\partial z},$$

where n_i is the number density of species i, φ_i the vertical flux, P_i the chemical production rate and L_i the chemical loss rate, all evaluated at time t and altitude z. The vertical flux is given by

$$\phi_i = -D_i\left(\frac{\partial n_i}{\partial z} + \frac{n_i}{H_i} + \frac{1-\alpha_i}{T}\frac{\partial T}{\partial z}n\right) - K\left(\frac{\partial n_i}{\partial z} + \frac{n_i}{H_a} + \frac{1}{T}\frac{\partial T}{\partial z}n\right),$$

where D_i is the species' molecular diffusion coefficient, H_i the species' scale height, H_a the atmospheric scale height, α_i the thermal diffusion parameter, K_{zz} the vertical eddy diffusion coefficient and T the temperature[50]. The flux consists of molecular diffusion (which can be derived from the molecular theory of ideal gases) and eddy transport. We calculate the eddy diffusion coefficient profile according to the formulation in ref. 51.

We assume a zero-flux upper and lower boundary condition for all species except the following: O (the rate of escape from the top via dissociative recombination is solved for in an iteration of KINETICS runs); O_2 (a ground deposition velocity of 2×10^{-6} cm^{-1} s^{-1} or fluxes of loss to the surface as described in the main text); H (the rate of thermal escape is solved for as described in the main text); H_2 (the rate of thermal escape is solved for and near-surface emissions are parametrized as described in the main text); HNO_2, HNO_3 and HO_2NO_2 (a ground deposition velocity of 10^{-2} cm^{-1} s^{-1}), CO (a ground deposition velocity of 10^{-6} cm^{-1} s^{-1}) and ion species (a zero concentration at the surface is considered).

We consider six atmospheric pressures and compositions: 200 mbar to 1.3 bar surface pressures, background CO_2 composition and up to 300 mbar N_2. This range is motivated by isotope evolution models and recent escape rate measurements. Reference 16 reports a median N_2 partial pressure of 310 mbar and ref. 52 reports a partial pressure of CO_2 of <1 bar in the Late Noachian. The latter agrees with extrapolations of present-day escape rates to early times (with adjustments for solar evolution) that suggest 0.8 bar CO_2 may have been lost to space[53]. Larger partial pressures for CO_2 would probably require larger amounts of carbonate formation than present-day measurements suggest[52,54]. It is possible deep subsurface carbonates are present, but since we have no evidence for them at the present, we ignore this possibility.

We solve for the thermal escape of hydrogen[55], escape of oxygen to dissociative recombination including electron impact ionization[56], and photochemical escape of carbon (according to ref. 57). We parametrize sputtering for carbon species[52] at the upper boundary condition, and we implement crustal hydration (in warm cases) or oxidant sinks (in cool cases) at the lower boundary condition. This is the first photochemical model with these mechanisms to be applied to early Mars. We do not include pick-up or other ion loss mechanisms as their modern-Mars loss rates are negligible for hydrogen, factors of several lower than photochemical escape for oxygen[53], and unknown for carbon, and because too much uncertainty exists in early solar system space weather conditions[46,58]. We assume a constant thermospheric temperature for ion profiles due to uncertainty in earlier times, but it is likely O escape rates would decrease due to decreased availability of CO_2 under higher thermospheric temperatures[59].

In the present-day atmosphere, water photolysis and subsequent HO_x chemistry drives hydrogen formation near the surface. Hydrogen escapes, both thermally after diffusing above the exobase[60] and non-thermally through photochemical reactions[61,62], with a thermal-to-non-thermal ratio of ~3. Oxygen escapes primarily via dissociative recombination of O_2^+ (the primary ionospheric constituent)[63]. At present day, the CO_2 content is regulated by similar HO_x chemistry, in which photolysis:

$$CO_2 + h\nu \rightarrow CO + O$$

is balanced by a recycling reaction:

$$CO + OH \rightarrow CO_2 + H.$$

We hypothesize the reduced iron in the crust modified this redox balance by crustal hydration in early warm climates with surface liquid water[13] to supply large hydrogen fluxes, or by acting as an oxidant sink in cool dry climates with limited surface liquid water[30].

The H_2 is formed primarily near the surface, where water photolysis is fast as water vapour becomes limited in the upper atmosphere due to cold trapping. We represent this in our model by assigning a constant H_2O mixing ratio (ratio, by volume, of water number density to total atmospheric number density) above the cold-trapped layer and assigning a mixing ratio that corresponds to the saturation vapour pressure of water at and below the cold-trapped layer (the first layer where the temperature profile becomes isothermal). At present-day Mars, humidity is variable on short timescales (<1 sol) but can reach values near 50–75% during the day and near saturation just before dawn at a few times of the year[64,65]. A wetter early Mars would have been more humid. Importantly, our results of zero H_2 flux coming from the ground show that photochemically derived H_2 (from this water) is orders of magnitude smaller than H_2 sourced from the ground (represented at the boundary conditions in the other cases). Thus, this assumption is negligible on our photochemical and climate results.

We find episodic geologic fluxes of $\geq 10^{12}$ H_2 cm^{-2} s^{-1} are required to sustain warm climates. These rates are within the order-of-magnitude estimates from ref. 12, whose experiments suggest an upper limit of 5×10^{12} H_2 cm^{-2} s^{-1} under an assumption that 10% of the early Mars surface may have hosted authigenic H_2 production. Similarly, ref. 26 suggests fluxes of up to 10^{13} H_2 cm^{-2} s^{-1} may be expected at slow-spreading ridges at Earth, although direct comparison to their work is difficult since conditions are warmer and host greater volumes of liquid water than likely at early Mars. Fluxes of $\geq 10^{12}$ H_2 cm^{-2} s^{-1} are larger than the crustal hydration fluxes presented in ref. 14, which estimated consistent time-averaged fluxes from crustal hydration over Mars's history. Their work still considered transient large fluxes but attributed episodicity to other events (including volcanism and impacts).

In cool climates, we vary the sink of atmospheric O_2 to oxidize the crust as a free parameter. Chemical rates for iron oxidation by O_2 have been measured at >1,000 K (ref. 66); however, the rate of iron oxidation by atmospheric oxidants is poorly constrained at temperatures relevant to the early Mars surface and are likely to be slow. We consider one case with no oxidant sinks as a basis for comparison. In this case, the photochemical results (Fig. 3) differ from the assumed warm scenarios (Fig. 2) because CO deposition to the ground is fixed to zero at the lower boundary in this cool climate (in warm climates, a small deposition velocity is applied to CO at the surface to represent consumption by

aqueous processes). With no sink to the ground, CO mixing ratios are of a few percent in the 1 bar atmosphere and are near 10% in thinner atmospheres. CO is more abundant in thinner atmospheres due to lower water availability.

The mechanism of a CO runaway may also be self-limiting. By losing O_2 and O_3 from the atmosphere, atmospheric oxidants (primarily OH) are eaten up in trying to replenish the reservoir of oxidized species. This loss of atmospheric oxidants depletes the system of OH and severely slows the recycling reaction CO + OH → CO_2 + H, yielding a CO-dominated atmosphere in cases of larger O_2 sinks. The loss of a CO_2-dominated atmosphere removes the main photochemical production pathway for O_2, effectively placing an upper limit on the rate of O_2 loss to oxidizing the surface. Therefore, large sinks of O_2 to the ground would probably not be sustained on long timescales of >10^8 years. The rate of iron oxidation by O_2 would scale with the abundance of O_2 and availability of reduced iron, so the loss rate of O_2 (which we prescribe and fix) would decrease over time as more O_2 is lost from the system and more iron becomes oxidized. Our KINETICS simulations show that CO begins to build up and O_2 begins to deplete after ~10^7 years, which is approximately the timescale this feedback would begin.

Catalytic chlorine chemistry is known to prevent a CO runaway at Venus (for example, ref. 31). The presence of present-day surface perchlorates (for example, ref. 39) and the potential for chlorates to oxidize ferrous iron at early Mars[67] also point to catalytic chemistry involving chlorine radicals as a means to prevent a CO runaway, as at Venus (for example, ref. 31). Cl chemistry would originate from volcanism. The lifetime of HCl at present-day Mars varies between 90 and 1,000 sols (ref. 68 0, whereas the timescale of a CO runaway is >10^7 years. Thus, Cl chemistry should be considered at Mars in future works, but to prevent a CO runaway, we predict repeated events would need to occur. In the main text, we pose that geologic events such as volcanism, meteorite impacts and/or obliquity changes may have helped prevent the CO runaway. Atmospheric collapse of CO_2 at Mars under different obliquity regimes has been considered by many previous works (for example, refs. 27,69), but we acknowledge obliquity changes remain highly uncertain, and some works suggest fewer events at both Mars (for example, ref. 70) and Earth (for example, ref. 71).

Radiative transfer model

REDFOX calculates radiative transfer for discrete intervals in the spectral range from ν = 0 to 10^5 cm^{-1}. We individually studied the temperature responses to including CO_2–H_2, H_2–H_2, as well as added N_2–H_2 CIA[72] in our scenarios, and even in the two cases of added 300 mbar of N_2 we found the N_2 to affect surface temperatures less than 2 K. Surface temperature changes between the five atmospheres considered are attributed mainly to variations in surface pressure opposed to the compositional variations. This is in agreement with ref. 9, which found that the more heterogeneous electron density distribution of the major atmospheric constituent CO_2 strengthens the multipole moments and increases the polarizability, leading to a stronger CIA effect compared with that of any added N_2. This result is in contrast to the early Earth study by ref. 73, which had found N_2–H_2 to significantly increase their temperatures. The difference lies mainly in the large amounts of CO_2 in early Mars, with major absorption bands in the same wavelength range as the N_2–H_2 CIA. See ref. 21 for a full list of atmospheric absorbers included in our correlated-*k* radiative transfer and for details about the cross sections. Water concentrations in convective regions in the troposphere are adjusted to follow modern Earth-like relative humidity profiles after ref. 74 with surface relative humidity = 0.77, including the potential presence of a liquid water ocean.

Data availability

KINETICS and REDFOX outputs and python scripts to generate Figs. 2–4 and Supplementary Fig. 1 are provided at https://doi.org/10.7910/DVN/QAEOFR.

Code availability

KINETICS was developed by a combination of authors (D.A. and Y.L.Y.) and many who are not co-authors on this work[15,49]. Per the KINETICS User Agreement, we do not have permission to distribute the source code, but an executable to reproduce the runs can be provided on reasonable request. REDFOX is IP of DLR Berlin, available to developer and co-author M.S. as a courtesy, but not available for public distribution. Outputs from the model are provided to the reader in 'Data availability'.

References

49. Nair, H. et al. A photochemical model of the Martian atmosphere. *Icarus* **111**, 124–150 (1994).
50. Yung, Y. L. & DeMore, W. B. *Photochemistry of Planetary Atmospheres* (Oxford Univ. Press, 1998).
51. Ackerman, A. S. & Marley, M. S. Precipitating condensation clouds in substellar atmosphere. *Astrophys. J.* **556**, 872 (2001).
52. Hu, R. et al. Tracing the fate of carbon and the atmospheric evolution of Mars. *Nat. Commun.* **6**, 10003 (2015).
53. Jakosky, B. et al. Loss of the Martian atmosphere to space: present-day loss rates determined from MAVEN observations and integrated loss through time. *Icarus* **315**, 146–157 (2018).
54. Jakosky, B. The CO_2 Inventory on Mars. *Planet. Space Sci.* **175**, 52–59 (2019).
55. Hunten, D. The escape of light gases from planetary atmospheres. *J. Atmos. Sci.* **30**, 1481–1494 (1973).
56. Lillis, R. et al. Ionization efficiency in the dayside ionosphere of Mars: structure and variability. *J. Geophys. Res. Planets* **126**, e2021JE006923 (2021).
57. Lo, D., Yelle, R. & Lillis, R. Carbon photochemistry at Mars: updates with recent data. *Icarus* **352**, 14001 (2020).
58. Wood, B., Muller, H., Zank, G., Linsky, J. & Redfield, S. New mass-loss measurements from astrospheric Lyα absorption. *Astrophys. J.* **628**, L143–L146 (2005).
59. Zhao, J., Feng, T., Yufang, N. & Xiaomeng, H. DR-induced escape of O and C from early Mars. *Icarus* **284**, 305–313 (2017).
60. Chaffin, M. et al. Mars H escape rates derived from MAVEN/IUVS Lyman alpha brightness measurements and their dependence on model assumptions. *J. Geophys. Res. Planets* **123**, 2192–2210 (2018).
61. Gregory, B. et al. Nonthermal hydrogen loss at Mars: contributions of photochemical mechanisms to escape and identification of key processes. *J. Geophys. Res. Planets* **128**, e2023JE007802 (2023).
62. Bhattacharyya, D. et al. Evidence of non-thermal hydrogen in the exosphere of Mars resulting in enhanced water loss. *J. Geophys. Res. Planets* **128**, e2023JE007801 (2023).
63. Lillis, R. et al. Photochemical escape of oxygen from Mars: first results from MAVEN in situ data. *J. Geophys. Res. Space Phys.* **122**, 3815–3836 (2017).
64. Harri, A.-M. et al. Pressure observations by the Curiosity rover: initial results. *JGR Planets* **119**, 82–92 (2014).
65. Polkko, J. et al. Initial results of the relative humidity observations by MEDA Instrument onboard the Mars 2020 Perseverance Rover. *GR Planets* **128**, e2022JE007447 (2023).
66. Abuluwefa, H. et al. The effect of oxygen concentration on the oxidation of low-carbon steel in the temperature range 1000 to 1250 °C. *Oxid. Met.* **46**, 423–440 (1996).
67. Mitra, K. et al. Formation of manganese oxides on early Mars due to active halogen cycling. *Nat. Geosci.* **16**, 133–139 (2023).
68. Aoki, S. et al. Annual appearance of hydrogen chloride on Mars and a striking similarity with the water vapor distribution observed by TGO/NOMAD. *Geophys. Res. Lett.* **48**, e2021GL092506 (2021).
69. Forget, F. et al. 3D modelling of the early Martian climate under a denser CO_2 atmosphere: temperatures and CO_2 ice clouds. *Icarus* **222**, 81–99 (2013).

70. Holo, S., Kite, E. & Robbins, S. Mars obliquity history constrained by elliptic crater orientations. *Earth Planet. Sci. Lett.* **496**, 206–214 (2018).
71. Lissauer, J., Barnes, J. & Chambers, J. Obliquity variations of a moonless Earth. *Icarus* **217**, 77–87 (2012).
72. Borysow, A. & Frommhold, L. Theoretical collision-induced rototranslational absorption spectra for modeling Titan's atmosphere: H_2–N_2 pairs. *Astrophys. J.* **303**, 495–510 (1986).
73. Wordsworth, R. & Pierrehumbert, R. Hydrogen-nitrogen greenhouse warming in Earthas early atmosphere. *Science* **339**, 64–67 (2013).
74. Manabe, S. & Wetherald, R. Thermal equilibrium of the atmosphere with a given distribution of relative humidity. *J. Atmos. Sci.* **24**, 241–259 (1967).

Acknowledgements

The data repository with KINETICS output data files is available at https://doi.org/10.7910/DVN/8JCR8U. We thank D. Lo, S. Stone, M. Wong and S. Bartlett for valuable discussions and for helpful suggestions to the manuscript. This project was supported in part by a Discovery Fund from Caltech Geological and Planetary Sciences and a Research and Technology Development Fund from JPL. D.A.'s research is funded by NASA through the NASA Hubble Fellowship Program Grant HST-HF2-51523.001-A awarded by the Space Telescope Science Institute, which is operated by the Association of Universities for Research in Astronomy, Inc., for NASA, under contract NAS5-26555. This work was supported in part by NASA Habitable Worlds grant NNN13D466T, later changed to 80NM0018F0612. R.H.'s research was carried out at the Jet Propulsion Laboratory, California Institute of Technology, under a contract with the National Aeronautics and Space Administration. T.B.T. acknowledges funding from the NSF GRFP (DGE-1762114) and the Virtual Planetary Laboratory, a member of NASA NExSS, funded via the NASA Astro-biology Program (grant 80NSSC18K0829). R.W. acknowledges funding from Leverhulme Center for Life in the Universe. The funders had no role in study design, data collection and analysis, decision to publish or preparation of the manuscript.

Author contributions

D.A. conceived the research question and KINETICS approach, adapted and ran KINETICS, analysed model output and drafted the manuscript. M.S. adapted and ran REDFOX and analysed model output. R.H. concepted interfacing with REDFOX, and analysed model output. B.L.E. provided concepts for geologic scenarios and fluxes. T.B.T. estimated H_2 outgassing rates by volcanism. E.S. contributed to geologic constraints for H_2 release. R.W. provided input and background on climate and geology. R.L. provided input on CO_2 photolysis and electron impact ionization. K.S. conducted HO_x sensitivity tests. H.R. contributed to REDFOX. Y.L.Y. developed original KINETICS code and analysed model output. All authors participated in writing and editing the manuscript.

Competing interests

The authors declare no competing interests.

Additional information

Supplementary information The online version contains supplementary material available at https://doi.org/10.1038/s41561-024-01626-8.

Correspondence and requests for materials should be addressed to Danica Adams.

Peer review information *Nature Geoscience* thanks James Kasting and the other, anonymous, reviewer(s) for their contribution to the peer review of this work. Primary handling editor: Tamara Goldin, in collaboration with the *Nature Geoscience* team.

Reprints and permissions information is available at www.nature.com/reprints.